




Original Article

## Radar Absorber Composite Graphene Oxide/Magnetite/Zinc Oxide in Polypyrrole Matrix

Allodya Nadra Xaviera<sup>1</sup>, Vania Agatha Nareswari<sup>1</sup>, Dea Dwi Ananda<sup>1</sup>, Hazzha Azzahra<sup>1</sup>, Thessa Octavia Joyetta Tarigan<sup>1</sup>, Tiara Rizki Yulita<sup>1</sup>, Nugroho Adi Sasongko<sup>2,3,4</sup>, Rahmat Basuki<sup>1\*</sup> 

<sup>1</sup>Department of Chemistry, The Republic of Indonesia Defense University, Kawasan IPSC Sentul, Bogor 16810, Indonesia

<sup>2</sup>Research Center For Sustainable Production System and Life Cycle Assessment, National Research and Innovation Agency (BRIN), KST Prof. BJ Habibie, Building 720 Puspiptek Area, South Tangerang, Banten 15314, Indonesia

<sup>3</sup>Energy Security Graduate Program, The Republic of Indonesia Defense University, Kawasan IPSC Sentul, Bogor 16810, Indonesia

<sup>4</sup>Murdoch University, 90 South St, Murdoch Western Australia 6150, Australia

<https://doi.org/10.55749/ss.v1i1.80>

Received: 27 May 2025; Revised: 4 Jun 2025; Accepted: 24 Jun 2025; Published online: 29 Jun 2025; Published regularly: 30 Jun 2025

This is an open access article under the CC BY-SA license (<https://creativecommons.org/licenses/by-sa/4.0/>).

**Abstract**— The development of stealth technology in modern defense systems demands superior radar absorbing material (RAM) innovation. This study aims to synthesize and characterize Fe<sub>3</sub>O<sub>4</sub>/ZnO modified carbon-based RAM composites in a polypyrrole (PPy) matrix using graphite oxide (GiO). The composites were synthesized via a modified Hummer method as well as a one-pot technique, and characterized using FTIR, XRD, SEM-EDX, and VNA. The FTIR characterization results showed that the C=C peak decreased in intensity after the oxidation process, indicating the breaking of the aromatic double bond and the formation of new functional groups such as C–O and C=O. This change was detected in both pGiO and kGiO samples. XRD data showed a shift in the main peaks to 2θ = 11.25° and 42.20° for pGiO and 2θ = 11.56° and 42.40° for GiO-k, respectively. This shift indicates the formation of a more amorphous graphite oxide structure compared to the original graphite. The results show that GiO/Fe<sub>3</sub>O<sub>4</sub>/ZnO has the highest reflection loss value of -9.20 dB at 10.91 GHz (GiO-p/Fe<sub>3</sub>O<sub>4</sub>/ZnO 66%-PPy) with an absorption value of 88.03% and rGO/Fe<sub>3</sub>O<sub>4</sub>/ZnO/PPy the highest RL value reached -7.51 dB at 11.57 GHz (rGO-k/Fe<sub>3</sub>O<sub>4</sub>/ZnO 66%-PPy) with an absorption value of 82.21%. This research proves that Fe<sub>3</sub>O<sub>4</sub>/ZnO modified carbon-based composites in a polypyrrole matrix have high potential as an efficient radar absorbing material and can support the needs of domestic defense technology.

**Keywords**— Carbon composite; Fe<sub>3</sub>O<sub>4</sub>/ZnO; Polypyrrol; Radar absorbing material; Stealth technology.

### 1. INTRODUCTION

In an effort to achieve independence in defense equipment production, the Defense Industry Policy Committee has formulated a national strategic program, which includes the development of indigenous radar technologies. One of the key innovations within this program is the advancement of stealth technology, which aims to reduce the detectability of objects by enemy radar systems [1]. This technology is implemented across various defense platforms, including fighter aircraft, bombers, helicopters, missiles, and submarines.

Stealth technology in military defense systems can be implemented through two primary approaches: modifying the structural design of the equipment to minimize radar wave reflection, and applying radar-absorbing coatings to the surface [2]. Structural modification typically involves substantial financial investment, making the use of absorbing materials a more cost-effective alternative. Radar wave absorption involves coating the surface of an object with materials that reduce the intensity of incoming electromagnetic waves by converting the absorbed radar energy into heat [3].

\*Corresponding author.

Email address: [rhmtbsq@gmail.com](mailto:rhmtbsq@gmail.com)

There are several criteria required for the development of radar absorbing materials, including ability to absorb electromagnetic waves up to low frequencies, minimizing radar visibility by reducing the effect of electromagnetic wave reflection, light and thin structure, good electrical conductivity and magnetic conductivity, high thermal stability, corrosion resistance, and easy to produce commercially [4]. The combination of dielectric and magnetic materials in RAM can enhance the performance and efficiency of electromagnetic wave absorption [2].

Magnetic materials which exhibit strong magnetic properties, are widely utilized as base materials for effective microwave absorbers, one of example is  $\text{Fe}_3\text{O}_4$  [5]. Magnetite is typically derived from iron sand and contains oxidized iron that forms iron oxide, a compound known for its strong magnetic characteristics [6]. Dielectric materials are materials that have ability to store and convert electrical energy under the influence of an electric field and are responsive to electromagnetic waves due to their low polarization and conductivity [7]. Dielectric materials function as RAM by mechanisms of polarization and relaxation loss [8], with commonly used examples including carbon-based materials [9], metal oxides, and polymers [10].

Carbon-based materials are known for their inertness, chemical stability, corrosion resistance, high electrical conductivity, and thermal stability across a wide range of temperatures [11]. These properties enable carbon materials to effectively absorb electromagnetic radiation within the S-band and X-band frequency ranges, typically between 2 and 12 GHz [11]. One of the carbon materials that has the potential to be developed as RAM is graphite oxide [12-13]. Graphite oxide exhibits an interconnected porous structure, a large specific surface area, and high potential for chemical modification, all of which contribute to enhanced electrical conductivity and electromagnetic wave absorption capabilities [14].

The synthesis of graphite and its derivatives commonly employs a top-down approach, which is generally regarded as efficient and cost-effective for producing high-quality materials [15]. One widely used top-down method is the modified Hummers method, which utilizes a mixture of sulfuric acid ( $\text{H}_2\text{SO}_4$ ), sodium nitrate ( $\text{NaNO}_3$ ), and potassium permanganate ( $\text{KMnO}_4$ ) as oxidizing agents [16]. During the oxidation of graphite, various oxygen-containing functional groups such as hydroxyl, epoxide, and carboxyl was formed [17].

In addition to carbon-based materials, metal oxides are also considered promising candidates for radar absorbing materials due to their strong affinity for oxygen anions and their tunable crystal structures [18]. These materials demonstrate the ability to interact with electromagnetic radiation in the gigahertz frequency range. Among various dielectric metal oxides, zinc oxide ( $\text{ZnO}$ ) has attracted significant attention.  $\text{ZnO}$  offers several advantages, including excellent dielectric properties, low density, and its function as a wide-bandgap semiconductor (3.37 eV). Moreover,  $\text{ZnO}$  also has structural stability at room temperature in the

hexagonal wurtzite phase, and can be synthesized economically on a large scale [19].

In this study, a polymer-based dielectric composite incorporating conductive polymers was utilized to enhance the performance of radar absorbing materials (RAM). Conductive polymers, such as polypyrrole (PPy), are capable of conducting electric current and possess unique properties that contribute to the reduction of electromagnetic wave reflection and absorption [20]. Polypyrrole exhibits high electrical conductivity, low specific gravity, flexibility, oxidation resistance, and can be synthesized through an efficient process. When used as a matrix in composites, PPy can be combined with inorganic materials to improve thermal stability and enhance electromagnetic wave absorption efficiency through the synergistic effects of dielectric properties and the porous structure of the composite [21].

Previous studies have demonstrated that RAM materials based on carbon/ $\text{Fe}_3\text{O}_4$ / $\text{ZnO}$  exhibit good absorption capabilities; however, they are limited by a relatively narrow effective absorption bandwidth (reflection loss,  $\text{RL} \leq -10$  dB), thereby restricting the range of electromagnetic frequencies that can be effectively absorbed [22]. The incorporation of PPy into the composite is expected to improve dielectric properties and electrical conductivity, thereby strengthening the electromagnetic wave attenuation mechanism through interfacial polarization and dipole relaxation. This enhancement is anticipated to broaden the absorption bandwidth and improve overall RAM performance.

The development of carbon-based radar absorbing materials (RAM) has been extensively explored using a variety of raw materials, including rice husks [23], cocoa pods [24], palm oil residues [25], and others. However, carbon derived from these sources generally exhibits low crystallinity, which may limit its effectiveness in electromagnetic wave absorption applications. In contrast, pencil-grade graphite represents a low-cost, widely available carbon source with high crystallinity [26]. Despite its potential, the application of pencil graphite as a RAM precursor remains relatively unexplored. This study aims to synthesize and characterize composites based on reduced graphene oxide–magnetite–zinc oxide ( $\text{rGO}/\text{Fe}_3\text{O}_4/\text{ZnO}$ ) and graphite oxide–magnetite–zinc oxide ( $\text{GiO}/\text{Fe}_3\text{O}_4/\text{ZnO}$ ), embedded within a polypyrrole (PPy) matrix. The incorporation of these components is expected to enhance the performance of RAM through improved electrical and magnetic properties, interfacial polarization, and synergistic loss mechanisms. The resulting composites are anticipated to exhibit optimized structural and electromagnetic characteristics, contributing to the development of high-efficiency RAM materials with superior radar wave absorption capabilities.

## 2. EXPERIMENTAL SECTION

### 2.1. Materials

The materials consist of graphite pencil, commercial graphite, and pure analytical chemical by Merck:  $\text{NaNO}_3$ ,  $\text{H}_2\text{SO}_4$ ,  $\text{KMnO}_4$ ,  $\text{HCl}$ ,  $\text{ZnCl}_2$ ,  $\text{FeCl}_3 \cdot 6\text{H}_2\text{O}$ ,  $\text{FeSO}_4 \cdot 7\text{H}_2\text{O}$ ,  $\text{NH}_4\text{OH}$ , Pyrrole, and hydrazine hydrate.

## 2.2. Instrumentation

The instrumentation includes FTIR-Prestige-21 Shimadzu, SEM-EDS ASTM, XRD D8 Advance (Bruker) Bragg-Bentano Diffraction, VNA Advantest R3770, Shimadzu analytical balance, sonicator, centrifugator, magnetic stirrer, oven, and hot plate stirrer. In addition, additional tools are needed such as funnels, conical bottles, Erlenmeyer flasks, measuring flasks, beakers, droppers, volume pipettes, measuring flasks, and watch glasses.

## 2.3. Preparation of Graphite Oxide (GiO) from Pencil and Commercial Graphite

The GiO synthesis using the modified Hummer method. The graphite used consisted of pencil graphite with a hardness level of 2B and commercial graphite in crystalline form (300 mesh, Alfa Aesar). 2 g of graphite, 50 mL of sulfuric acid ( $\text{H}_2\text{SO}_4$  98%), and 0.5 g of  $\text{NaNO}_3$ . The solution was stirred at  $5^\circ\text{C}$  for 30 minutes at a speed of 300 rpm. Gradually, 6 g of  $\text{KMnO}_4$  were added and stirred for 3 hours at a constant temperature and stirring speed in an ice bath. During the process, the solution will change color from solid black to greenish black. After the reaction was complete, 100 mL of water was slowly added to the mixture for 1 hour at temperature  $50^\circ\text{C}$  and a stirring with 300 rpm. Then, 10 mL of hydrogen peroxide ( $\text{H}_2\text{O}_2$ ) 30% was added to the mixture and stirred for 30 minutes at temperature  $50^\circ\text{C}$  and stirring with 300 rpm. The mixture was separated using Büchner vacuum until a solid was obtained. The solid was rinsed with 80 mL of 20%  $\text{HCl}$  followed by distilled water until a neutral pH was achieved. Then the obtained solid was dried in an oven at a temperature of  $110^\circ\text{C}$  for 12 hours. The synthesis of GiO from commercial graphite was carried out with the same procedure as the synthesis of GiO from pencil graphite. All samples were characterized by XRD and FTIR.

## 2.4. Synthesis of ZnO

A total of 0.5 g  $\text{ZnCl}_2$  dissolved in 25 mL of distilled water, stirred for 1 hour at temperature  $40^\circ\text{C}$ . Then  $\text{NH}_4\text{OH}$  was added into the solution and the pH was maintained at 11–13 while stirring at a stable speed for 10 min.

## 2.5. Synthesis of Graphene Oxide/Magnetite/Zinc Oxide ( $\text{GiO}/\text{Fe}_3\text{O}_4/\text{ZnO}$ )

A total of 0.5 g of pencil graphite GiO was dissolved in 60 mL deionized water by ultrasonication for 30 minutes.  $\text{Fe}^{2+}/\text{Fe}^{3+}$  solution was prepared by dissolving  $\text{FeCl}_3 \cdot 6\text{H}_2\text{O}$  and  $\text{FeSO}_4 \cdot 7\text{H}_2\text{O}$  in 5 mL of distilled water (11.5 mmol/3.1 g: 5.625 mmol/1.575 g). The  $\text{Fe}^{2+}/\text{Fe}^{3+}$  solution was mixed into the GiO solution. Temperature

was maintained at  $90^\circ\text{C}$ . After the temperature was reached, the ZnO solution was added while continuing stirrer. The solution was washed with deionized water (DI). Then the solid was calcined at  $300^\circ\text{C}$  for 3 h. The  $\text{GiO}/\text{Fe}_3\text{O}_4/\text{ZnO}$  composites were synthesized using both pencil graphite and commercial graphite following the same procedure. The resulting samples were characterized using SEM-EDS, XRD, and FTIR analyses.

## 2.6. Synthesis $\text{GiO}/\text{Fe}_3\text{O}_4/\text{ZnO}$ Composite

A total of 0.25 g (20%); 0.50 g (33%); and 2 g (66%) of  $\text{GiO}/\text{Fe}_3\text{O}_4/\text{ZnO}$  were dissolved in 60 mL aquadest. Then, 0.21 mL of monomer pyrrole was added to the solution. The mixture was sonicated for 1 h and reacted with 2.4 g  $\text{FeCl}_3$  dissolved in 0.1 M  $\text{HCl}$ , slowly. The mixture was stirred for 4 h. The obtained samples were filtered and washed with aquadest-ethanol and then dried in an oven at  $110^\circ\text{C}$  for 10 h. All samples were characterized using FTIR, XRD, SEM-EDS, and VNA at a thickness of 1.5 mm.

## 3. RESULT AND DISCUSSION

### 3.1. Characterization of GiO from Pencil and Commercial Graphite

The synthesis process of graphite oxide (GiO) was carried out using the Hummers method. In this study, two types of graphite precursors were used, namely pencil graphite (p) and commercial graphite (k). The initial stage involved the process of sieving graphite to a size of 100 mesh to equalize the surface area, thus facilitating the homogenization process. Furthermore, graphite was mixed with sodium nitrate ( $\text{NaNO}_3$ ), concentrated sulfuric acid ( $\text{H}_2\text{SO}_4$ ) and potassium permanganate ( $\text{KMnO}_4$ ). The role of  $\text{NaNO}_3$  is to reduce the number of layers and slightly increase the distance between layers in graphite, and  $\text{H}_2\text{SO}_4$  functions to help the entry of oxidizer ions into the graphite structure and as a graphite solvent [27]. Meanwhile,  $\text{KMnO}_4$  was added gradually to initiate the oxidation process on both types of graphite. This reaction was carried out with constant stirring on an ice bath to control the temperature and prevent excessive exothermic reactions. During the addition of  $\text{KMnO}_4$ , the solution changed color to dark brown indicating that the graphite oxidation process had begun [27]. After oxidation takes place,  $\text{H}_2\text{O}_2$  is added to stop the oxidation reaction and reduce the remaining  $\text{KMnO}_4$  [28]. The addition of  $\text{H}_2\text{O}_2$  causes the colour of the solution to change to greenish brown, which indicates the successful completion of the oxidation process.

FTIR analysis is used to confirm that the oxidized graphite has formed graphite oxide with the presence of spectrum changes in FTIR. The analysis is carried out by comparing the functional group spectra between pencil graphite (Gi-p), pencil GiO (GiO-p), commercial graphite (Gi-k), and commercial GiO (GiO-k). From the

results of the FTIR analysis, a graph is obtained which can be seen in **Figure 1**.

The results of the FTIR spectrum data show that the characteristic peaks of Gi-p, Gi-k, GiO-p, and GiO-k indicating the presence of C=C groups in stretching vibrations were detected in all samples. This indicates that the material has a  $sp^2$  hybridization type (triangular planar) [29]. Based on **Figure 1**, the Gi-p sample only has a C=C group at the  $1589\text{ cm}^{-1}$  absorption peak and a C-O group at the  $1059\text{ cm}^{-1}$  peak. The presence of the C-O spectrum indicates that the graphite material has undergone a carbonation or pyrolysis process [30]. Therefore, it is confirmed that the pencil graphite has undergone a carbonation or pyrolysis process.

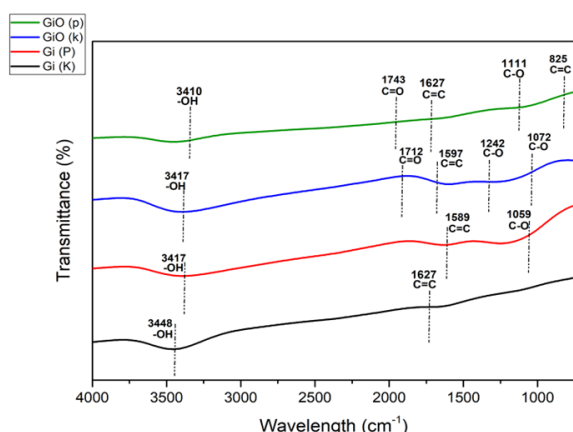


**Figure 1.** FTIR spectra of Gi-p, Gi-k, GiO-p, and GiO-k

The GiO-p sample shows several oxygen groups indicating that the graphite oxidation process with the modified Hummer method took place well according to previous studies [31]. The typical functional group in graphite oxide is epoxy, but GiO-p does not contain intercalated epoxy groups due to the type of  $sp^2$  hybridization having minimal plane defects [32].

The functional groups in the Gi-k sample show that they only have C=C groups at the absorption peak of  $1627\text{ cm}^{-1}$  (**Figure 1**). The increase in absorption intensity in the C=O, C-O, and -OH groups shows that the oxidation process from Gi-k to GiO-k using the modified Hummer method has been going well [33]. The oxidation process successfully intercalated oxygen groups in the graphite layer and caused significant structural changes [34].

Then, GiO-p and GiO-k materials have the presence of C=C groups indicating that in graphite conditions there are still carbon double bonds in the aromatic structure, but due to the oxidation and heating process the aromatic structure is broken and oxygen functional groups are formed [35]. It can also be seen that the presence of -OH bonds was detected in all samples. This bond is likely derived from KBr used in making pellets. KBr is hygroscopic and easily soluble in water, so it can absorb water molecules from the surrounding environment [35].

### 3.2. XRD Analysis Results of GiO from Gi-p and Gi-k

The analysis was carried out using XRD instrument by identifying each diffraction pattern of Gi-p, Gi-k, GiO-k, and GiO-p. The test was carried out using X-ray using an angle range of  $10^\circ$ - $90^\circ$  and a wavelength of  $1.54056\text{ \AA}$ . The X-ray diffraction pattern of XRD spectrum is shown in **Figure 2**.

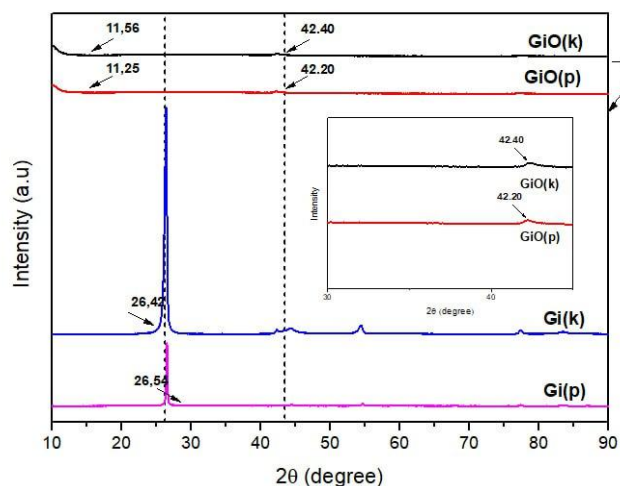


**Figure 2.** Diffraction patterns of Gi-p, GiO-p, Gi-k, and GiO-k

Analysis of the XRD data pattern shows that the crystallinity of Gi-k is higher compared to Gi-p. This is indicated by the sharper diffraction peak at  $2\theta = 26.42^\circ$  for Gi-k compared to Gi-p at  $2\theta = 26.54^\circ$ . This is in line with the highly ordered layer structure along the (002) plane with d-spacing values of  $3.37\text{ \AA}$  for Gi-k and  $3.35\text{ \AA}$  for Gi-p, respectively. This is in line with the highly ordered layer structure along the (002) plane, with d-spacing values of  $3.37\text{ \AA}$  for Gi-k and  $3.35\text{ \AA}$  for Gi-p, respectively. This shift in the XRD angle pattern indicates a change in the crystallinity properties of the graphite material. After the oxidation process, it can be observed that the graphite oxide samples, both in Gi-k and Gi-p show a tendency towards the amorphous phase. This is indicated by the emergence of wider diffraction peaks. Comparison of the crystallinity of Gi-k, Gi-p, GiO-k, and GiO-p was 86.2%, 71.9%, 23.4%, and 21.1%, respectively.

The degree of crystallinity of Gi-k shows the highest level of crystallinity, which is 86.2%, while Gi-p has a lower crystallinity, which is 71.9%. This difference shows that commercial graphite has a more regular layer arrangement compared to graphite pencils. After the oxidation process, there was a significant decrease in crystallinity in both types of graphite. The crystallinity of Gi-k decreased drastically to 23.4%, while Gi-p decreased to 21.1%. The decrease in crystallinity occurred because the modified Hummer method used in the oxidation process resulted in damage to the crystal structure which triggered disruption to the inner layer of graphite oxide [35].

These changes in properties can also be confirmed through X-ray diffraction (XRD) patterns, where after oxidation, the diffraction peaks broaden, and their

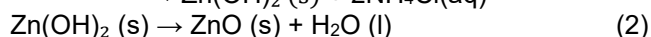
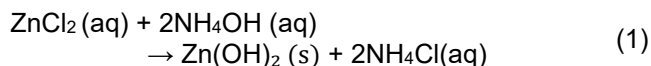


intensity decreases significantly. In GiO-p the main peak shifts to  $2\theta = 11.25^\circ$  (001) and  $42.20^\circ$  (100) and GiO-k to  $2\theta = 11.56^\circ$  (001) and  $42.40^\circ$  (100) from the diffraction pattern it can be seen that there is a peak shift from Gi to GiO and indicates the presence of an amorphous phase in graphite oxide. The shift of the (002) plane angle to a lower angle to the (001) plane at an angle of  $2\theta = 11.25^\circ$  as a typical peak in GiO is in accordance with the reference data (JCPDS Card No.75-1621), this indicates that there is a significant structural change due to the oxidation process. The presence of a peak around  $2\theta = 19.90^\circ$  indicates that graphene is in the form of a stack of layers and not as a monolayer [36]. This decrease indicates that oxidation causes changes in the graphite structure to become more irregular due to the entry of oxygen groups into the graphite layer. The presence of these oxygen groups disrupts the interaction between layers and increases the distance between planes (d-spacing), increasing d-spacing to 7.65 Å in GiO-k and 7.86 Å in GiO-p. This proves that graphite has undergone oxidation and turned into graphite oxide [37].

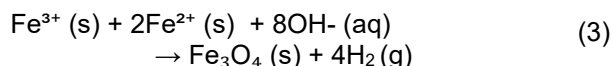
The formation of the amorphous phase is also an indicator of the formation of graphite oxide. In addition, the high carbon intensity is closely related to the increase in the amorphous phase in the material. Thus, these results as a whole confirm that graphite has been successfully oxidized into graphite oxide.

### 3.3. Synthesis of GiO/Fe<sub>3</sub>O<sub>4</sub>/ZnO Composite

The synthesis stages of modified carbon composites with Fe<sub>3</sub>O<sub>4</sub>/ZnO were carried out in stages. The first was the synthesis of GiO-p and GiO-k on Fe<sub>3</sub>O<sub>4</sub>/ZnO using the one-pot method, with precursors ZnCl<sub>2</sub>, FeCl<sub>3</sub>·6H<sub>2</sub>O, and FeSO<sub>4</sub>·7H<sub>2</sub>O. In the initial stage, ZnO synthesis was carried out. ZnCl<sub>2</sub> was first dissolved in distilled water to ionize Zn<sup>2+</sup>, thus facilitating the subsequent reaction process. After that, the solution was reacted with NH<sub>4</sub>OH, which produced Zn (OH)<sub>2</sub> precipitate, indicated by a change in the solution to become slightly cloudy. Homogenization was carried out for 30 minutes at a temperature of 40°C with heating, causing the solution to become transparent. This process shows that Zn (OH)<sub>2</sub> is dehydrated and transformed into ZnO due to the presence of sufficient heat energy and water molecules [38]. The reaction that occurs can be seen in the Equation (1) and (2).



Then, the previously dispersed solution was combined with Fe<sup>2+</sup>/Fe<sup>3+</sup> solution and heated to 90°C. At this temperature, co-precipitation of Fe<sup>2+</sup> and Fe<sup>3+</sup> ions occur, which allows the optimal formation of Fe<sub>3</sub>O<sub>4</sub> (Equation 3).



The process of adding ZnCl<sub>2</sub>/NH<sub>4</sub>OH is carried out to accelerate the formation of Fe<sub>3</sub>O<sub>4</sub>, which occurs under alkaline conditions and heating to 90°C. At this stage, the solution begins to thicken, so it is necessary to stir for 1 h at a constant temperature so that perfect homogenization can be achieved. The final result is a black suspension. The solid obtained is then tested with a magnet, which indicates the success of the synthesis of GiO/Fe<sub>3</sub>O<sub>4</sub>/ZnO. Furthermore, the GiO/Fe<sub>3</sub>O<sub>4</sub>/ZnO solid is composited with polypyrrole. The composite material is synthesized through a one-pot stage by combining oxidative polymerization, where the Fe<sup>3+</sup> ion acts as an oxidizer for pyrrole. Graphene oxide (GO) contains many functional groups such as carboxyl and hydroxyl. When the pyrrole monomer is added to the GO solution, the pyrrole easily adheres to the GO surface due to the hydrogen bond interaction between the N-H groups in the polymer and the oxygen groups on GO. This interaction forms a nucleation center that supports the in-situ polymerization of polypyrrole (PPy) [39]. FeCl<sub>3</sub> acts as an effective oxidizer for pyrrole, so that after FeCl<sub>3</sub> is added, pyrrole polymerization takes place directly on the GO surface.

### 3.4. FTIR Analysis Results of GiO/Fe<sub>3</sub>O<sub>4</sub>/ZnO

FTIR was used to confirm the functional groups of GiO/Fe<sub>3</sub>O<sub>4</sub>/ZnO from pencil and commercial graphite. The analysis was carried out by comparing the functional group spectrum of modified carbon with Fe<sub>3</sub>O<sub>4</sub>/ZnO (Figure 3).

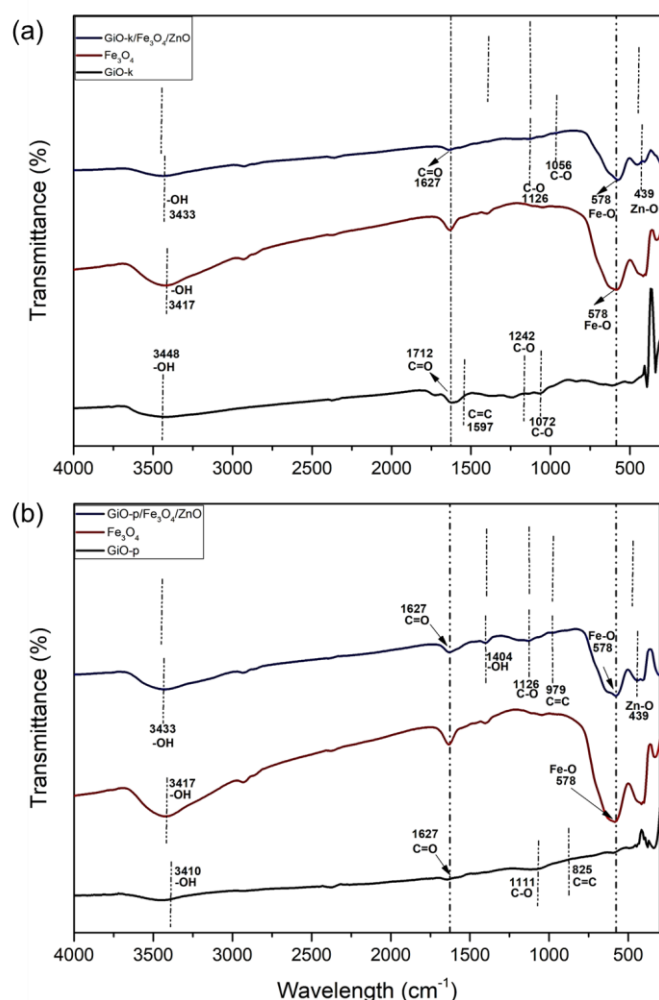


**Figure 3.** FTIR spectrum of (a) GiO-p/Fe<sub>3</sub>O<sub>4</sub>/ZnO, and (b) GiO-k/Fe<sub>3</sub>O<sub>4</sub>/ZnO

It is confirmed that GiO-p/Fe<sub>3</sub>O<sub>4</sub>/ZnO contains several oxygen-containing functional groups, namely hydroxyl, alcohol, and carbonyl in its structure. It can be seen that the results of the FTIR spectrum show that all samples have a characteristic peak at 578 cm<sup>-1</sup> which indicates the formation of Fe<sub>3</sub>O<sub>4</sub>. The absorption peak in the range of 578–610 cm<sup>-1</sup> indicates the presence of vibrations from the Fe-O bond [40].

Then, the presence of ZnO in all materials was confirmed through the absorption peak at 439 cm<sup>-1</sup>. According to previous studies, the absorption peak at around 400–500 cm<sup>-1</sup> indicates the presence of Zn-O bonds [41]. The presence of the Zn-O absorption peak indicates a chemical interaction between Zn metal oxide and GiO during the functionalization process [42]. In addition, it can be seen that another absorption that appears in the 1404 cm<sup>-1</sup> area is thought to originate from the -OH bond formed in the modified carbon material with Fe<sub>3</sub>O<sub>4</sub>/ZnO both in pencils and graphite. Based on previous studies, the absorption that appears around 1395 cm<sup>-1</sup> indicates the presence of bending vibrations of water molecules attached to the carbon plane [43]. Meanwhile, the absorption bands that appear in all samples around 3418 and 3433 cm<sup>-1</sup> are associated with the presence of characteristic

absorption from the -OH group which indicates the presence of hydrogen bonds between the materials [44]. Based on the analysis results, this indicates that there is a chemical bond and strong interaction between GiO-p/Fe<sub>3</sub>O<sub>4</sub>/ZnO and GiO-k/Fe<sub>3</sub>O<sub>4</sub>/ZnO.

The difference between pencil graphite and commercial graphite explained by the C=C absorption peak in pencil graphite at 979 cm<sup>-1</sup>, while in commercial graphite it is lower, around 972 cm<sup>-1</sup>. Another difference is the disappearance of the -OH peak in commercial graphite indicating high purity. This shows that the source of graphite affects the structure and composition of functional groups in the synthesized material.

### 3.5. XRD Analysis Results of Fe<sub>3</sub>O<sub>4</sub>/ZnO Modified Carbon

Analysis of Fe<sub>3</sub>O<sub>4</sub>/ZnO modified carbon was carried out through XRD test by identifying each diffraction pattern of GiO/Fe<sub>3</sub>O<sub>4</sub>/ZnO. The test was carried out using X-rays in the angle range of 10°– 90° with a wavelength of 1.54056 Å. The X-ray diffraction pattern was analyzed based on the XRD spectrum of pencil graphite and commercial graphite, as shown in **Figure 4**.

The diffraction pattern of X-rays shows the change of crystalline structure after the modification process. The GiO-p and GiO-k samples show diffraction patterns with low intensity and broad peaks, indicating that the samples are amorphous or have low crystallinity. The black dashed line in the Figure indicates the formation of graphite oxide in the material mixture. Then carbon is combined with Fe<sub>3</sub>O<sub>4</sub>, it can be seen that Fe<sub>3</sub>O<sub>4</sub> has a special peak with the highest intensity at 2θ = 35.560, 57.720, 62.880, corresponding to the crystal planes (311), (511), and (440) which are in accordance with JCPDS (96-900-745) [45].

The XRD diffraction pattern of GiO-p/Fe<sub>3</sub>O<sub>4</sub>/ZnO sample shows several main diffraction peaks detected at angles 2θ = 18.20°, 30.20°, 35.60°, 43.21°, 57.22°, 74.40°, and 75.31°. This diffraction pattern shows amorphous characteristics characterized by the presence of non-sharp peaks and resembles the diffraction pattern of amorphous materials. Changes in GiO-p, after mixing with Fe<sub>3</sub>O<sub>4</sub>/ZnO, there is a shift in the diffraction angle from 2θ = 19.77° with a d-spacing value of 4.48 Å to 2θ = 18.20° with a d-spacing value of 4.87 Å, which indicates a change in the crystal structure. This shift can be attributed to the interaction between GiO-p with Fe<sub>3</sub>O<sub>4</sub> and ZnO, which indicates a change in the distance between crystal planes (d-spacing).

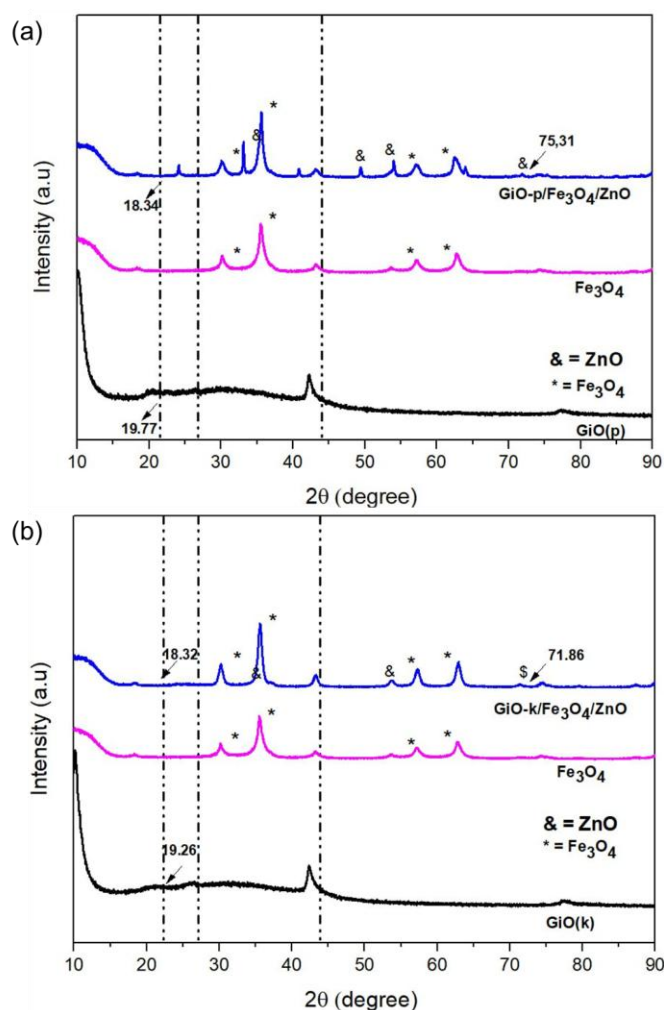


**Figure 4.** Diffraction Pattern of (a) GiO-p/Fe<sub>3</sub>O<sub>4</sub>/ZnO, and (b) GiO-k/Fe<sub>3</sub>O<sub>4</sub>/ZnO

The presence of ZnO is confirmed by the emergence of distinctive peaks at  $2\theta = 49.43^\circ$  (102) and  $75.31^\circ$  (202), which correspond to the wurtzite structure of ZnO in the hexagonal phase [45]. The weak peak value of ZnO is due to the deposition in thin sheets on graphite [46]. In its crystal structure, ZnO adopts the wurtzite crystal structure, namely the hexagonal lattice arrangement of Zinc and Oxygen atoms [47].

The crystallinity degree of the GiO-k (23.4%), Fe<sub>3</sub>O<sub>4</sub> (65%), and GiO-k/Fe<sub>3</sub>O<sub>4</sub>/ZnO (72.7%) show that GiO-k/Fe<sub>3</sub>O<sub>4</sub>/ZnO has a diffraction pattern similar to pencil graphite, with relatively similar values. However, when compared with commercial graphite, the crystallinity results of the pencil are higher than commercial graphite.

Comparison the crystallinity degree of GiO-k and GiO-p shows that GiO-k higher than that of GiO-p. The crystallinity of GiO-k has a value of 23.4%, while GiO-p has a lower crystallinity, which is 21.1%. After the mixing process with Fe<sub>3</sub>O<sub>4</sub>/ZnO, the crystallinity of both increases, but GiO-k/Fe<sub>3</sub>O<sub>4</sub>/ZnO still has a higher crystallinity (72.7%) than GiO-p/Fe<sub>3</sub>O<sub>4</sub>/ZnO (70.9%). The crystal size of Fe<sub>3</sub>O<sub>4</sub>, GiO-k/Fe<sub>3</sub>O<sub>4</sub>/ZnO, GiO-p/Fe<sub>3</sub>O<sub>4</sub>/ZnO were 62.15, 59.69, and 57.28 nm, respectively. Fe<sub>3</sub>O<sub>4</sub> is the highest crystallite size, so that when GiO-p and GiO-k are mixed with Fe<sub>3</sub>O<sub>4</sub>/ZnO, there

is a phase change into crystals with the following average crystal sizes.

The increase in crystallinity is due to Fe<sub>3</sub>O<sub>4</sub> acting as a nucleation center that allows carbon atoms in graphite to rearrange their arrangement [48]. In addition, the interaction between Fe<sub>3</sub>O<sub>4</sub> and ZnO with GiO can increase the structural stability and atomic order in the material formed. With ZnO material that has a wurtzite structure, it can play a role in increasing directional crystal growth so that crystallinity increases [49]. When reduction is carried out on graphite, the reduction changes the structure of graphite oxide because there are oxygen groups that are removed and allow C atoms to reform a more regular sp<sup>2</sup> structure [50]. It can be concluded that commercial graphite (Gi-k) has higher crystallinity than pencil graphite (Gi-p) because its layer structure is more regular. However, after modification, the possibility of irregular crystallinity is caused by an imperfect synthesis process and becomes an impurity [51].

### 3.6. FTIR Analysis Results of GiO/Fe<sub>3</sub>O<sub>4</sub>/ZnO-Ppy Composition Variations

The results of FTIR analysis were used to confirm the functional groups of GiO/Fe<sub>3</sub>O<sub>4</sub>/ZnO with various ratios of pencil graphite and commercial graphite that had been composited with polypyrrole. FTIR analysis was carried out by comparing the functional group spectrum of Fe<sub>3</sub>O<sub>4</sub>/ZnO modified carbon composites to obtain information on bond changes so that results were obtained regarding the presence of functional groups formed and the effect of modification on the structure and properties of the resulting composite.

The results of the FTIR spectrum for each material in pencil graphite can be seen in **Figure 5a**. Through functional group analysis, it can be ascertained that the spectrum formed in the GiO-p/Fe<sub>3</sub>O<sub>4</sub>/ZnO/Ppy composite is a combination of the GiO-p/Fe<sub>3</sub>O<sub>4</sub>/ZnO and Ppy spectra, which indicates that the particles in the composite have good homogeneity during the synthesis process. In addition, it can be ascertained that the GiO-p/Fe<sub>3</sub>O<sub>4</sub>/ZnO particles are well dispersed in Ppy [52]. Various compositions of GiO-p/Fe<sub>3</sub>O<sub>4</sub>/ZnO with Ppy it can be seen that the effect on the spectrum with the addition of variations of GiO-p/Fe<sub>3</sub>O<sub>4</sub>/ZnO, the spectrum absorption intensity decreased. This happens because the addition of material can disrupt the PPy conjugation structure, so that the bonds in the polymer become weaker [53].



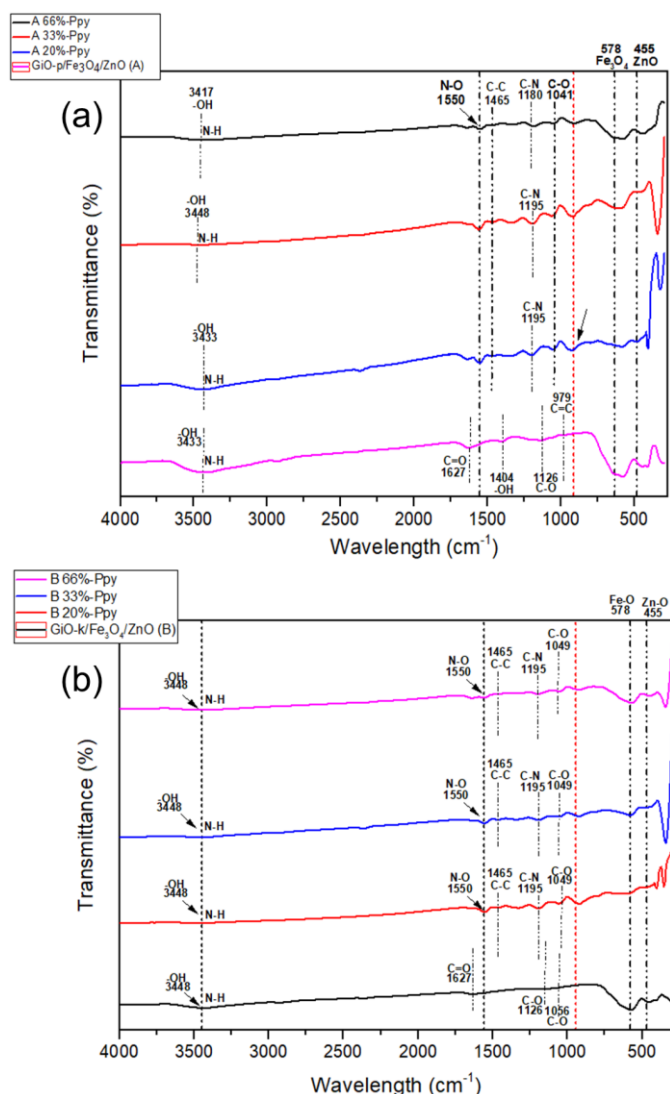


**Figure 5.** FTIR spectrum of various compositions of (a) GiO-p/Fe<sub>3</sub>O<sub>4</sub>/ZnO/Ppy and (b) GiO-k/Fe<sub>3</sub>O<sub>4</sub>/ZnO/Ppy

Through FTIR analysis, it is confirmed that GiO-p/Fe<sub>3</sub>O<sub>4</sub>/ZnO/Ppy contains several functional groups containing nitrogen in the form of nitro and amine. There is a red dotted line indicated by the arrow at the peak of the spectrum around 925 cm<sup>-1</sup> indicating that there is an out-of-plane ring deformation related to the movement of the pyrrole ring structure that is not in one plane, this indicates that there is a conformational change due to interaction with other materials [54]. With the addition of variations of GiO-p/Fe<sub>3</sub>O<sub>4</sub>/ZnO, the intensity of the FTIR spectrum decreases, which means that the bonds and interactions between the material and the composite are getting weaker. For comparison, FTIR analysis was carried out on GiO-k/Fe<sub>3</sub>O<sub>4</sub>/ZnO. The results of the FTIR spectrum for each material in commercial graphite can be seen in **Figure 5b**. The results obtained, similar to GiO-p/Fe<sub>3</sub>O<sub>4</sub>/ZnO/Ppy, the GiO-k/Fe<sub>3</sub>O<sub>4</sub>/ZnO material contains a number of nitrogen functional groups, namely nitro and amine. The difference is only seen from the absorption intensity which has a difference that is not much different. With this, it can be concluded that the polymerization process of Ppy occurs with the

appearance of nitro and amine groups and a shift in the FTIR spectrum indicating that the GiO p/Fe<sub>3</sub>O<sub>4</sub>/ZnO/Ppy and GiO-k/Fe<sub>3</sub>O<sub>4</sub>/ZnO/Ppy materials were successfully synthesized [55].

The FTIR spectrum results show that all samples have characteristic peaks at 578-609 cm<sup>-1</sup>, which indicates the formation of Fe<sub>3</sub>O<sub>4</sub>, based on previous studies in the range of 578–610 cm<sup>-1</sup> indicating the presence of vibrations from the Fe-O bond [56]. With this absorption band indicating the presence of a cubic spinel structure in the Fe-O bond. Then it can be seen that the FTIR spectrum of the Zn-O bond in all materials has an absorption peak of around 455 cm<sup>-1</sup>. According to previous studies, the absorption peak at around 400-500 cm<sup>-1</sup> indicates the presence of a Zn-O bond [57].

The FTIR spectrum results of the composite show the presence of typical absorption peaks at 1195, 1041, 1550 cm<sup>-1</sup> which are related to the presence of stretching vibrations in the C-N, C-O, and N-O groups. The characteristics of the C-N group indicate a typical band in the pyrrole ring, and a typical peak that broadens in the C-C bond indicates the formation of a Ppy composite [58]. Then, the presence of a spectrum peak of 3417-3433 cm<sup>-1</sup> is associated with the overlap between the -OH and -NH stretches which indicate the presence of hydroxyl groups and nitrogen-containing groups. The changes that occur in the peak position and band broadening from GiO/Fe<sub>3</sub>O<sub>4</sub>/ZnO to GiO/Fe<sub>3</sub>O<sub>4</sub>/ZnO-Ppy (p) indicate that there is a chemical interaction between the materials which causes the polymer conformation.

Analysis of functional groups shows the differences between pencil graphite and commercial graphite (**Figure 5**). It can be seen that the FTIR peak absorption of both graphites has almost the same typical pattern. This indicates that there has been an interaction between GiO-p/Fe<sub>3</sub>O<sub>4</sub>/ZnO and Ppy as well as GiO-k/Fe<sub>3</sub>O<sub>4</sub>/ZnO and Ppy. The peak shift and the emergence of new absorption bands indicate the presence of chemical bonds between these components. In addition, changes in intensity and peak broadening in the C=O and C=C regions indicate that the graphite structure has been modified due to interaction with other materials. Thus, based on the FTIR analysis, it can be concluded that the GiO-p/Fe<sub>3</sub>O<sub>4</sub>/ZnO/Ppy and GiO-k/Fe<sub>3</sub>O<sub>4</sub>/ZnO/Ppy composites have been successfully formed.

### 3.7. XRD Analysis Results of Composition Variation of GiO/Fe<sub>3</sub>O<sub>4</sub>/ZnO/Ppy

Analysis of Fe<sub>3</sub>O<sub>4</sub>/ZnO modified carbon composites on Ppy was carried out through XRD by identifying each diffraction pattern. The test was carried out using X-rays in the angle range of 10°-90° with a wavelength of 1.54056 Å. The XRD pattern was used to compare the crystallinity properties of Fe<sub>3</sub>O<sub>4</sub>/ZnO modified carbon composites with various ratios and polypyrrole (Ppy). The ratio variation was obtained by adding GiO/Fe<sub>3</sub>O<sub>4</sub>/ZnO from pencil graphite and commercial in different amounts.



The XRD pattern for the Ppy-GiO-p/Fe<sub>3</sub>O<sub>4</sub>/ZnO composite can be seen in **Figure 6**. Based on the results obtained, there are several typical diffraction patterns in each material. From the composite, a high diffraction pattern intensity was obtained at around  $2\theta = 30^\circ, 35^\circ, 57^\circ, 62^\circ$  angles with planes (220), (311), (311), (440) which are similar to the Fe<sub>3</sub>O<sub>4</sub> material according to JCPDS (96-900-745) [59].

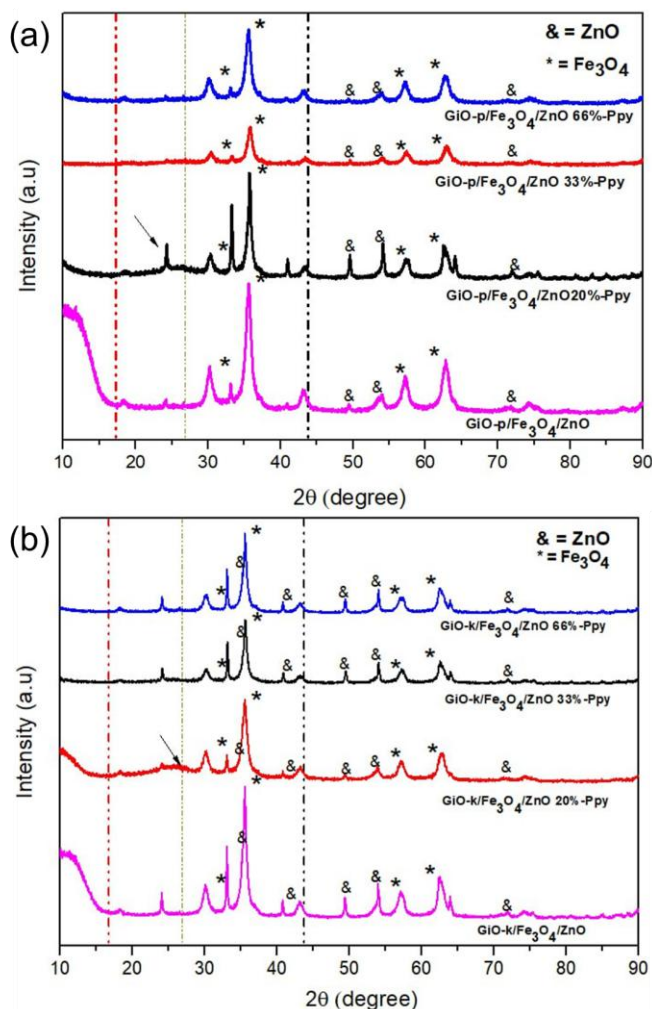


**Figure 6.** Diffraction pattern of (a) GiO-p/Fe<sub>3</sub>O<sub>4</sub>/ZnO/Ppy and (b) GiO-p/Fe<sub>3</sub>O<sub>4</sub>/ZnO/Ppy composition variation

The typical diffraction peaks of ZnO were observed around the angles of  $2\theta = 57^\circ$  (110) and  $75^\circ$  (202), which correspond to the wurtzite structure of ZnO in the hexagonal phase [60]. Based on previous studies, the diffraction intensity of ZnO/Ppy will show weak and broad XRD peaks due to the small distribution of ZnO and particle size. Based on previous studies, the diffraction intensity of ZnO/Ppy will show weak and broad XRD peaks due to the small distribution of ZnO and particle size.

From the peak obtained at the arrow, a diffraction peak is observed at an angle of  $2\theta = 24.27^\circ$ , indicating the presence of Ppy. Ppy has a peak at around  $15^\circ < 2\theta < 30^\circ$  which likely overlaps with the GiO peak. The resulting polypyrrole produces a sharp and long peak, meaning that the resulting Ppy interacts with the sheets

of graphite oxide to form a crystal structure [61]. After the addition of Ppy to GiO-p/Fe<sub>3</sub>O<sub>4</sub>/ZnO, it can be seen in the red dotted line that there is a change in the characteristics of the material which becomes more amorphous and the graph shifts slightly to the right indicating a change in the crystal lattice parameters, which can be caused by the interaction between Ppy and GiO-p/Fe<sub>3</sub>O<sub>4</sub>/ZnO. The results of the differences in composition variations in GiO-p/Fe<sub>3</sub>O<sub>4</sub>/ZnO can be seen in the degree of crystallinity as in **Table 1**.

**Table 1.** Crystallinity degree of GiO-p/Fe<sub>3</sub>O<sub>4</sub>/ZnO/Ppy and GiO-p/Fe<sub>3</sub>O<sub>4</sub>/ZnO/Ppy composition variation

Sample	Crystallinity Degree (%)
GiO-p/ Fe <sub>3</sub> O <sub>4</sub> /ZnO	70.90
GiO-p/ Fe <sub>3</sub> O <sub>4</sub> /ZnO 20%-Ppy	63.60
GiO-p/ Fe <sub>3</sub> O <sub>4</sub> /ZnO 33%-Ppy	60.80
GiO-p/ Fe <sub>3</sub> O <sub>4</sub> /ZnO 66%-Ppy	61.60
GiO-k/Fe <sub>3</sub> O <sub>4</sub> /ZnO	72.70
GiO-k/Fe <sub>3</sub> O <sub>4</sub> /ZnO 20%-Ppy	60.80
GiO-k/Fe <sub>3</sub> O <sub>4</sub> /ZnO 33%-Ppy	67.80
GiO-k/Fe <sub>3</sub> O <sub>4</sub> /ZnO 66%-Ppy	70.80

It can be seen that the addition of the composition of GiO-p/Fe<sub>3</sub>O<sub>4</sub>/ZnO to Ppy will reduce the crystallinity of the material. This can be explained based on the interaction between GiO-p, Fe<sub>3</sub>O<sub>4</sub>, ZnO, and Ppy, which causes changes in the crystalline structure in the composite. Ppy interacting with graphite will reduce crystallinity due to the more amorphous polypyrrole structure [62]. In GiO p/Fe<sub>3</sub>O<sub>4</sub>/ZnO 20%-Ppy, crystallinity is still relatively high (63.60%) with a crystal size of 50.48 nm. When the composition of GiO-p/Fe<sub>3</sub>O<sub>4</sub>/ZnO 33%-Ppy, there is a more significant decrease in crystallinity, which is 60.80%. This occurs because the distribution is uneven in the material, causing disruption of the crystal structure and reducing crystallinity. In this composition, the crystal size is 45.68 nm. However, at the composition of 66% GiO p/Fe<sub>3</sub>O<sub>4</sub>/ZnO, there was a slight increase in crystallinity compared to the variation of 33%, which was 61.60%. The increase occurred due to the possibility of aggregation in the particles, thereby reducing the gap between the materials and making the structure denser. This is evidenced by the crystal size of GiO-p/Fe<sub>3</sub>O<sub>4</sub>/ZnO 66%-Ppy which has a crystal size of 64.63 nm. The crystal size is larger but there is more irregularity in the crystal structure.

For comparison, XRD analysis was also carried out on the composition variation of GiO-k/Fe<sub>3</sub>O<sub>4</sub>/ZnO/Ppy. The XRD pattern of the composite can be seen in **Figure 6**. The analysis results show that the GiO k/Fe<sub>3</sub>O<sub>4</sub>/ZnO/Ppy composite has the same pattern as GiO-p/Fe<sub>3</sub>O<sub>4</sub>/ZnO/Ppy. However, there is a difference in the crystallinity of the two materials. The degree of crystallinity of the GiO-k/Fe<sub>3</sub>O<sub>4</sub>/ZnO/Ppy composite can be observed as follows,

The results of the analysis showed that increasing the composition of GiO-k/Fe<sub>3</sub>O<sub>4</sub>/ZnO increased the crystallinity of the composite. The sharp peaks in the diffraction pattern indicate that the graphene oxide sheets play a role in increasing the crystalline structure

of polypyrrole [60]. The even dispersion of materials in the composite and the dominance of the crystalline phases of ZnO and  $\text{Fe}_3\text{O}_4$  also contribute to the increase in crystallinity. In addition, based on the results of the crystallinity degree analysis, it can be concluded that commercial graphite has a higher degree of crystallinity compared to graphite from pencils.

### 3.8. SEM-EDX Characterization of $\text{Fe}_3\text{O}_4/\text{ZnO}$ Modified Carbon Composite on Ppy

Characterization using SEM-EDX was used to analyze the surface of GiO on  $\text{Fe}_3\text{O}_4/\text{ZnO}$  modified carbon composite samples on PPy. SEM characterization was used to describe the surface morphology of GO, while EDX characterization was used to obtain an overview of the carbon and oxygen content in the GiO material. **Figure 7** shows the surface morphology of pGiO/ $\text{Fe}_3\text{O}_4/\text{ZnO}$  at x10000 magnification shows the presence of smooth surface sheets and grains. Based on previous studies, the surface folds of GiO show a denser and less porous structure.

To confirm the success of the synthesis, EDX analysis was also carried out on each material. The EDX spectra of GiO-p/ $\text{Fe}_3\text{O}_4/\text{ZnO}$  are shown in **Figure 7c**. The GiO-k/ $\text{Fe}_3\text{O}_4/\text{ZnO}$  material shows a smooth surface sheet and grains. It can be seen that on the surface of the material there is quite significant agglomeration between the  $\text{Fe}_3\text{O}_4$  and ZnO particles attached to the GiO sheet. This agglomeration is caused by the high

magnetic properties of  $\text{Fe}_3\text{O}_4$ , which encourages the particles to interact with each other and form aggregates due to the attractive force between the particles. In addition, the observed agglomeration is also related to the relatively thin thickness of the ZnO layer, so that it is unable to completely block the interaction between particles. Based on previous studies, the addition of a larger amount of ZnO is known to help reduce agglomeration by forming a thicker protective layer on the particle surface [61].

Then, EDX analysis was carried out to analyze the success of the synthesis of GiO-p into rGO-p. The EDX spectrum of the GiO-p/ $\text{Fe}_3\text{O}_4/\text{ZnO}$  sample is shown in **Figure 7c**. The oxygen element (O) in GiO-p/ $\text{Fe}_3\text{O}_4/\text{ZnO}$  has a high intensity. The weight percentage of carbon and oxygen elements in GiO are 20.01% and 34.32%. In addition, the EDX spectrum on GiO-p/ $\text{Fe}_3\text{O}_4/\text{ZnO}$  shows that the Fe element has a high intensity and Zn has a low intensity. Based on the composition results, the weight of the Fe and Zn elements is 42.76% and 2.91%, while in rGO-p/ $\text{Fe}_3\text{O}_4/\text{ZnO}$  the weight of the Fe and Zn elements is 36.82% and 2.69%. This is related to proving that the material has more Fe atoms than Zn, causing agglomeration. The magnetic properties of  $\text{Fe}_3\text{O}_4$  encourage particles to interact with each other and form aggregates [61]. The EDX spectrum in **Figure 7d** shows that the oxygen element (O) in GiO-k/ $\text{Fe}_3\text{O}_4/\text{ZnO}$  has a high intensity. Meanwhile, the EDX

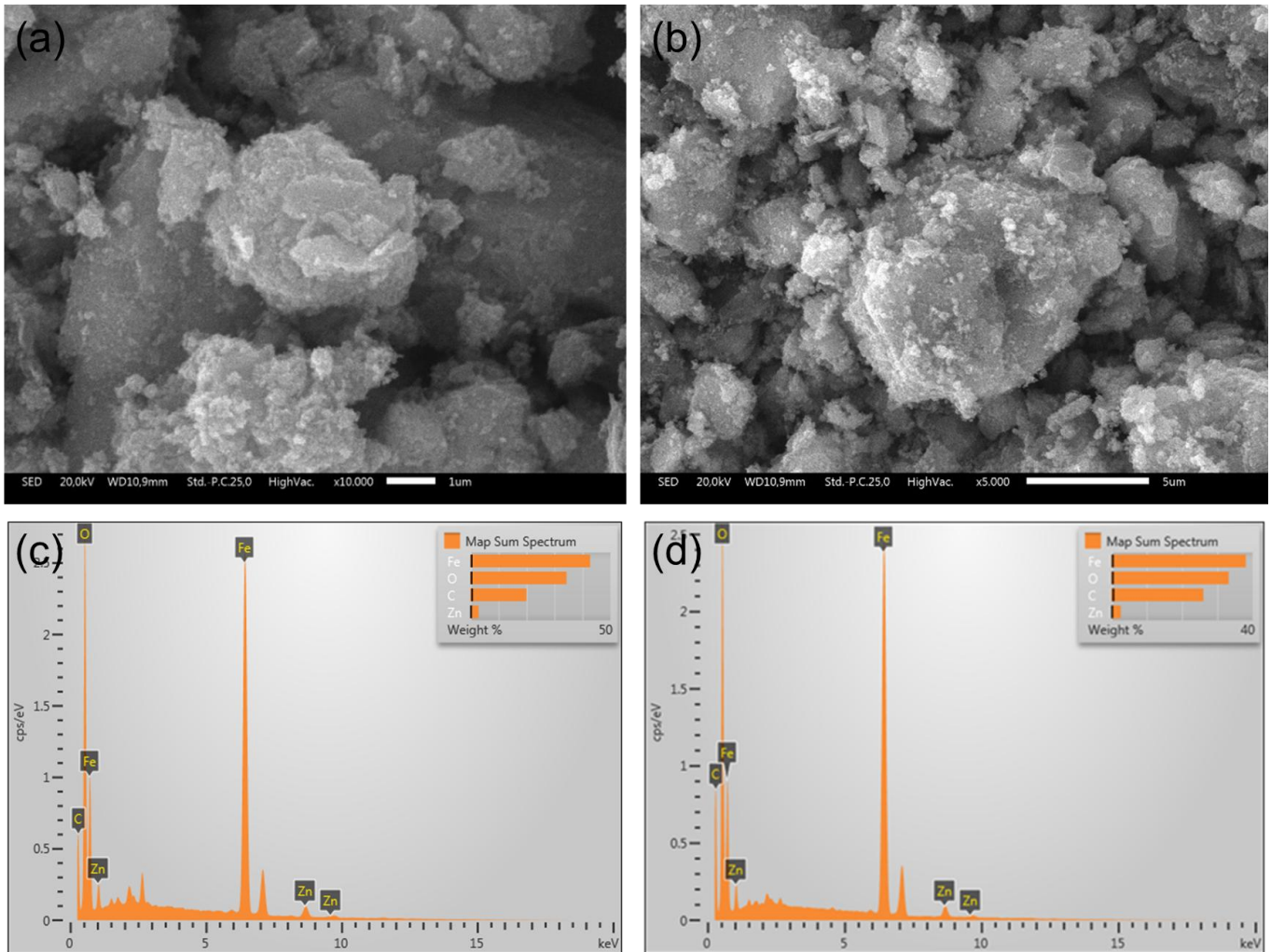


**Figure 7.** SEM results of (a) GiO-p/Fe<sub>3</sub>O<sub>4</sub>/ZnO (10000× magnification) and (b) GiO-k/Fe<sub>3</sub>O<sub>4</sub>/ZnO (5000× magnification), and EDX result of (c) GiO-p/Fe<sub>3</sub>O<sub>4</sub>/ZnO and (d) GiO-k/Fe<sub>3</sub>O<sub>4</sub>/ZnO

spectrum shows relatively similar results to pencil-based graphite.

### 3.9. Identification of Electromagnetic Wave Absorption Properties of Composites

Testing using a Vector Network Analyzer (VNA) will provide information on the characteristics of electromagnetic waves in the material, namely the reflection loss value and the amount of absorption power [62]. Reflection loss (RL in decibels (dB)) is the amount of energy reflected by an object or surface that is hit by a wave. A high reflection loss value indicates the amount of energy reflected while a low value indicates the amount of energy absorbed by a material [62].

The test was carried out on a 1 mm thick material placed between probes S11 (reflection wave) and S21 (transmission wave). Waves with a frequency range of 8–12 GHz were sent through probe 1 and received by probe 2. By using a probe adapter, the reflection, transmission, and absorption values of the sample can be obtained, which are then used to determine the reflection loss (RL) value. RL measurements on a 1 mm thick composite layer were carried out using a Vector Network Analyzer (VNA) type Advantest R3770, which

has a frequency range of 300 kHz–20 GHz. This test was carried out in the X-band frequency range (8–12 GHz) using a WR90 type waveguide. The results of VNA testing on Fe<sub>3</sub>O<sub>4</sub>/ZnO modified carbon composites with various ratios and polypyrrole (Ppy) can be seen in **Figure 8**.

Based on **Table 2**, the reflection loss value of GiO/Fe<sub>3</sub>O<sub>4</sub>/ZnO/PPy material from pencil graphite and commercial graphite is obtained. In GiO-p/Fe<sub>3</sub>O<sub>4</sub>/ZnO 20%-PPy, the reflection loss value is -4.62 dB at a frequency of 8.81 GHz. Meanwhile, GiO-p/Fe<sub>3</sub>O<sub>4</sub>/ZnO 33%-PPy shows a reflection loss of -5.76 dB at a frequency of 8.92 GHz, and GiO-p/Fe<sub>3</sub>O<sub>4</sub>/ZnO 66%-PPy has the highest reflection loss value of -9.20 dB at a frequency of 10.91 GHz. Based on the results obtained, it can be seen that the more GiO-p/Fe<sub>3</sub>O<sub>4</sub>/ZnO is added, the more the material's ability to absorb radar waves will increase. Similar results were also seen in the GiO-k/Fe<sub>3</sub>O<sub>4</sub>/ZnO/PPy composite. In GiO-k/Fe<sub>3</sub>O<sub>4</sub>/ZnO 20%-PPy has an RL value of -4.49 dB at a frequency of 8.75 GHz. Meanwhile, GiO-k/Fe<sub>3</sub>O<sub>4</sub>/ZnO 33%-PPy has a reflection loss of -4.95 dB at a frequency of 8.37 GHz. The highest results were obtained in GiO-k/Fe<sub>3</sub>O<sub>4</sub>/ZnO 66%-PPy, with a reflection loss value of -8.01 dB at a



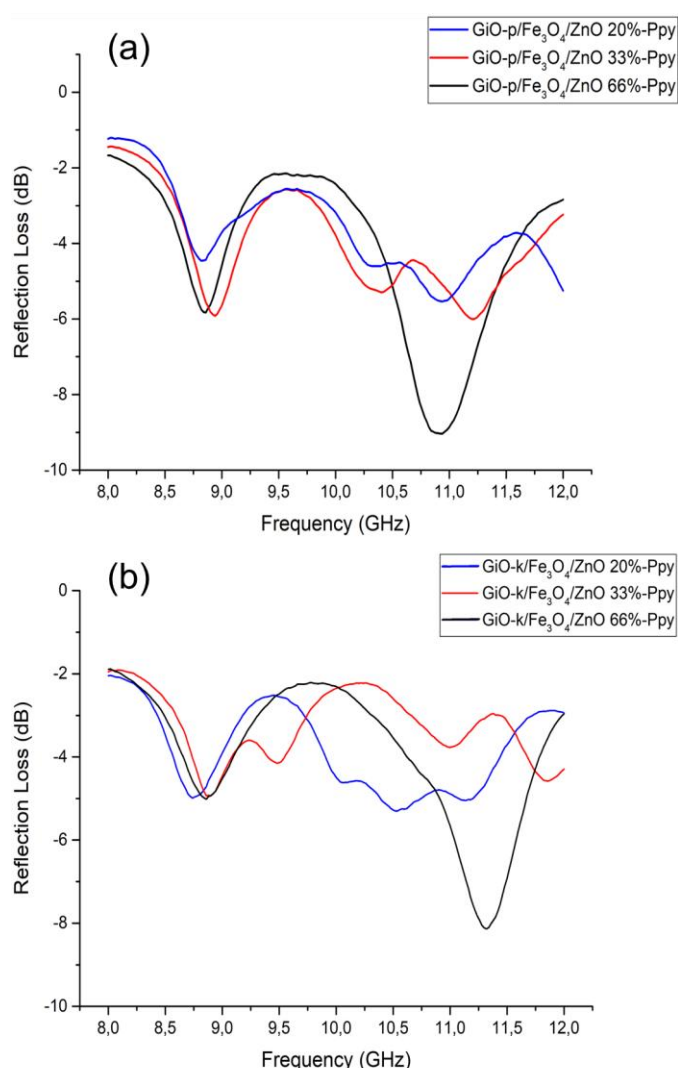


**Figure 8.** VNA Test Results on (a) GiO-p/Fe<sub>3</sub>O<sub>4</sub>/ZnO/PPy and (b) GiO-k/Fe<sub>3</sub>O<sub>4</sub>/ZnO/PPy

**Table 2.** Comparison of reflection loss values in gio based composite materials

Material	RL (dB)	Frequency (GHz)	Thickness (mm)
pGiO/Fe <sub>3</sub> O <sub>4</sub> /ZnO 20%-PPy	-4.62	8.81	1.5
pGiO/Fe <sub>3</sub> O <sub>4</sub> /ZnO 33%-PPy	-5.76	8.92	1.5
pGiO/Fe <sub>3</sub> O <sub>4</sub> /ZnO 66%-PPy	-9.20	10.91	1.5
kGiO/Fe <sub>3</sub> O <sub>4</sub> /ZnO 20%-PPy	-4.49	8.75	1.5
kGiO/Fe <sub>3</sub> O <sub>4</sub> /ZnO 33%-PPy	-4.95	8.87	1.5
kGiO/Fe <sub>3</sub> O <sub>4</sub> /ZnO 66%-PPy	-8.01	11.32	1.5
GiO/Zn/Fe <sub>2</sub> O <sub>4</sub> /Epoxy [63]	12.70	10.50	2.35
GiO [64]	-8.50	10.60	2.28
GiO/FeCoB/Epoxy [65]	10.98	8.45	2.00

frequency of 11.32 GHz. Based on these results, it can be seen that the more the composition of GiO-k/Fe<sub>3</sub>O<sub>4</sub>/ZnO is added, the more the material's ability to absorb radar waves will increase. Comparison between the two types of materials shows that GiO-p/Fe<sub>3</sub>O<sub>4</sub>/ZnO/PPy has a better RL value than GiO-k/Fe<sub>3</sub>O<sub>4</sub>/ZnO/PPy. The difference in RL values is associated with the crystallite size of each sample. The

crystallite size of GiO-p/Fe<sub>3</sub>O<sub>4</sub>/ZnO 66%-PPy reaches 65.50 nm, while GiO-k/Fe<sub>3</sub>O<sub>4</sub>/ZnO 66%-PPy is only 52.20 nm. For other compositions, GiO-p/Fe<sub>3</sub>O<sub>4</sub>/ZnO 33%-PPy has a crystallite size of 43.35 nm and GiO-p/Fe<sub>3</sub>O<sub>4</sub>/ZnO 20%-PPy is 63.68 nm. Meanwhile, GiO-k/Fe<sub>3</sub>O<sub>4</sub>/ZnO 33%-PPy has a size of 42.83 nm and GiO-k/Fe<sub>3</sub>O<sub>4</sub>/ZnO 20%-PPy is 66.03 nm. Based on previous studies, decreasing the crystal size can increase the maximum RL value [64].

#### 4. CONCLUSION

GiO/Fe<sub>3</sub>O<sub>4</sub>/ZnO material was successfully synthesized using the modified Hummer method confirmed by analysis using FTIR and XRD. GiO/Fe<sub>3</sub>O<sub>4</sub>/ZnO/PPy material composite was successfully synthesized as evidenced by analysis using FTIR and XRD. The results of the VNA analysis showed that GiO/Fe<sub>3</sub>O<sub>4</sub>/ZnO had the highest RL value of -9.20 dB at 10.91 GHz (rGiO-k/Fe<sub>3</sub>O<sub>4</sub>/ZnO 66%-PPy) with 88.03% absorption value.

#### SUPPORTING INFORMATION

There is no supporting information in this paper. The data that support the findings of this study are available on request from the corresponding author (R. Basuki).

#### ACKNOWLEDGEMENTS

The authors highly appreciate the FTIR and XRD characterization support provided by BRIN.

#### CONFLICT OF INTEREST

The authors have no conflict of interest in this publication.

#### AUTHOR CONTRIBUTIONS

ANX performed the conceptualization, investigation, methodology, writing original draft, review & editing. RB & NAS supervises the experiment, data calculations, and revise the manuscript. VA, DDA, HA, TOJT, and TRY collaborated on writing and revising the manuscript. All authors approved the final version of the manuscript.

#### REFERENCES

- [1] Abharya, A. & Gholizadeh, A. 2021. Synthesis of a Fe<sub>3</sub>O<sub>4</sub>-rGO-ZnO-Catalyzed photo-fenton system with enhanced photocatalytic performance. *Ceram. Int.* 47(9). 12010–12019. Doi: <https://doi.org/10.1016/j.ceramint.2021.01.044>
- [2] Admojo, L. & Setyawan, B. 2018. potensi pemanfaatan lignoselulosa dari biomasa kayu karet (*Hevea Brasiliensis* Muell Arg.). *Warta Perkaretan.* 37(1). 39–50. Doi: <https://doi.org/10.22302/ppk.wp.v37i1.529>
- [3] Aini, N.N., Widyastuti, W. & Fajarin, R. 2016. pengaruh jenis polimer terhadap reflection loss pada polymer matrix composite (PMC) barium heksaferit sebagai radar absorbing material (RAM). *Jurnal Teknik ITS.* 5(2). F125-F129. Doi: <https://doi.org/10.12962/j23373539.v5i2.17710>
- [4] Atay, H.Y. 2016. A comparison on radar absorbing properties of nano and micro-scale barium hexaferrite powders reinforced polymeric composites. *Mugla Journal of Science and Technology.* 2(1). 88–92. Doi: <https://doi.org/10.22531/muglajsci.269979>



- [5] Atay, H.Y. & Liqin, Ö. 2020. manufacturing radar-absorbing composite materials by using magnetic co-doped zinc oxide particles synthesized by sol-gel. *J. Compos. Mater.* 54(26). 4059–4066. Doi: <https://doi.org/10.1177/0021998320927754>
- [6] Batool, A., Kanwal, F., Imran, M., Jamil, T. & Siddiqi, S.A. 2012. Synthesis of polypyrrole/zinc oxide composites and study of their structural, thermal and electrical properties. *Synth. Met.* 161(23–24). 2753–2758. Doi: <https://doi.org/10.1016/j.synthmet.2011.10.016>
- [7] Baumgartner, J., Dey, A., Bomans, P.H., Le Coadou, C., Fratzl, P., Sommerdijk, N.A. and Faivre, D. 2013. Nucleation and growth of magnetite from solution. *Nat. Mater.* 12(4). 310–314. Doi: <http://dx.doi.org/10.1038/nmat3558>
- [8] Bhuvaneswari, S., Pratheeksha, P.M., Anandan, S., Rangappa, D., Gopalan, R. and Rao, T.N. 2014. Efficient reduced graphene oxide grafted porous Fe<sub>3</sub>O<sub>4</sub> composite as a high performance anode material for Li-ion batteries. *Phys. Chem. Chem. Phys.* 16(11). 5284–5294. Doi: <https://doi.org/10.1039/C3CP54778G>
- [9] Bolilanga, P.I.W., Basuki, R., Apriliyanto, Y.B., Prasajo, A.E., Lazuardy, A., Anitasari, R., Putri, R., Sasongko, N.A. and Santiko, A.B., Immobilization of Cerium (IV) oxide onto reduced graphene oxide in epoxy resin matrix as radar absorbing composite for x-band region. *Indones. J. Chem.* 24(6). 1688–1700. Doi: <http://dx.doi.org/10.22146/ijc.94404>
- [10] Chakradhary, V.K., Juneja, S. & Akhtar, M.J. 2020. Correlation between EMI shielding and reflection loss mechanism for carbon nanofiber/epoxy nanocomposite. *Mater. Today Commun.* 25. 101386. Doi: <https://doi.org/10.1016/j.mtcomm.2020.101386>
- [11] Chen, X., Qu, Z., Liu, Z. and Ren, G. 2022. Mechanism of oxidation of graphite to graphene oxide by the hummers method. *ACS Omega.* 7(27). 23503–23510. Doi: <https://doi.org/10.1021/Acsomega.2c01963>
- [12] Chieng, B.W., Ibrahim, N.A., Wan Yunus, W.M.Z. and Hussein, M.Z. 2013. Poly (lactic acid)/poly (ethylene glycol) polymer nanocomposites: Effects of graphene nanoplatelets. *Polymers.* 6(1). 93–104. Doi: <https://doi.org/10.3390/polym6010093>
- [13] Chieng, B.W., Ibrahim, N.A., Wan Yunus, W.M.Z., Hussein, M.Z., Then, Y.Y. and Loo, Y.Y. 2014. Effects of graphene nanoplatelets and reduced graphene oxide on poly (lactic acid) and plasticized poly (lactic acid): A comparative study. *Polymers.* 6(8). 2232–2246. Doi: <https://doi.org/10.3390/polym6082232>
- [14] Dawn, R., Zzaman, M., Faizal, F., Kiran, C., Kumari, A., Shahid, R., Panatarani, C., Joni, I.M., Verma, V.K., Sahoo, S.K. and Amemiya, K. 2022. Origin of magnetization in silica-coated Fe<sub>3</sub>O<sub>4</sub> nanoparticles revealed by soft X-ray magnetic circular dichroism. *Braz. J. Phys.* 52(3). 99. Doi: <http://dx.doi.org/10.1007/s13538-022-01102-x>
- [15] Du, Y., Pei, M., He, Y., Yu, F., Guo, W. & Wang, L. 2014. Preparation, characterization and application of magnetic Fe<sub>3</sub>O<sub>4</sub>-CS for the adsorption of orange I from aqueous solutions. *PloS one.* 9(10). e108647. Doi: <https://doi.org/10.1371/journal.pone.0108647>
- [16] Elmahaishi, M.F., Azis, R.A.S., Ismail, I., Matori, K.A. & Muhammad, F.D., 2024. Influence of particle size on the magnetic and microwave absorption properties of magnetite via mechano-mechanical methods for micro-nano-spheres. *Nano-Struct.* 39. 101207. Doi: <https://doi.org/10.1016/J.Nanoso.2024.101207>
- [17] Fischer, D., Zagorac, D. & Schön, J.C. 2023. Fundamental insight into the formation of the zinc oxide crystal structure. *Thin Solid Films.* 782. 140017. Doi: <https://doi.org/10.1016/j.tsf.2023.140017>
- [18] Ganash, E.A., Al-Jabarti, G.A. & Altuwirqi, R.M. 2019. The synthesis of carbon-based nanomaterials by pulsed laser ablation in water. *Mater. Res. Express.* 7(1). 15002. Doi: <http://dx.doi.org/10.1088/2053-1591/ab572b>
- [19] Hanifah, N., Hidayat, N., Yoghathi, C.I., Adi, W.A., Amrillah, T., Abd Aziz, M.S. & Taufiq, A. 2024. A novel Fe<sub>3</sub>O<sub>4</sub>/ZnO/PANI/rGO nanohybrid material for radar wave absorbing. *Mater. Chem. Phys.* 317. 129169. Doi: <https://doi.org/10.1016/j.matchemphys.2024.129169>
- [20] Ickecan, D., Zan, R. And Nezir, S. 2017. Eco-friendly synthesis and characterization of reduced graphene oxide. *J. Phys. Conf. Ser.* 12027. Doi: <http://dx.doi.org/10.1088/1742-6596/902/1/012027>
- [21] Jayswal, S. & Moirangthem, R.S. 2018. Thermal decomposition route to synthesize ZnO nanoparticles for photocatalytic application. *AIP Conf. Proc.* 2009(1). 020023. Doi: <https://doi.org/10.1063/1.5052092>
- [22] Johan, A., Adi, W.A., Arsyad, F.S., Ramlan, R. & Setiabudidaya, D. 2023. Comparative study of reflection loss of microwave absorbing materials from single phase Co<sub>1-x</sub>Zn<sub>x</sub>Fe<sub>2</sub>O<sub>4</sub> and CoFe<sub>2</sub>O<sub>4</sub>/LaFeO<sub>3</sub> composites. *AIP Conf. Proc.* 2913(1). 050005. Doi: <https://doi.org/10.1063/5.0171720>
- [23] Kim, S.H., Lee, S.Y., Zhang, Y., Park, S.J. & Gu, J. 2023. Carbon-based radar absorbing materials toward stealth technologies. *Adv. Sci.* 10(32). 2303104. Doi: <https://doi.org/10.1002/Adv.202303104>
- [24] Shalaby, A., Nihtianova, D., Markov, P., Staneva, A.D., Iordanova, R.S. & Dimitriev, Y.B., 2015. Structural analysis of reduced graphene oxide by transmission electron microscopy. *Bulg. Chem. Commun.* 47(1). 291–295.
- [25] Li, H., Yang, S., Zhao, Y., Tan, T., Wang, X. & Bakenov, Z. 2019. Synthesis of ZnO/Polypyrrole nanoring composite as high-performance anode materials for lithium ion batteries. *J. Nanomater.* 2019(1). 4702849. Doi: <https://doi.org/10.1155/2019/4702849>
- [26] Lia, Y., Zhao, B., Fan, S., Liang, L., Zhou, Y., Wang, R., Guo, X., Fan, B. & Zhang, R., 2019. ZnO amounts-dependent electromagnetic wave absorption capabilities of Ni/ZnO composite microspheres. *J. Mater. Sci.: Mater. Electron.* 30(22). 19966–19976. Doi: <https://doi.org/10.1007/s10854-019-02363-0>
- [27] Lv, H., Li, Y., Jia, Z., Wang, L., Guo, X., Zhao, B. & Zhang, R., 2020. Exceptionally porous three-dimensional architectural nanostructure derived from CNTs/graphene aerogel towards the ultra-wideband EM absorption. *Compos. B: Eng.* 196. 108122. Doi: <https://doi.org/10.1016/j.compositesb.2020.108122>
- [28] Mahadevi, V., Veeresh, S., Vijaykumar, B.T., Kolhar, P., Basavaraj, B. & Sannakki, B. 2024. Situ synthesis and characterization of polypyrrole/ZnO Nanocomposites for optical and photocatalytic activity. *IOP Conf. Ser. Mater. Sci. Eng.* 1300(1). 012022. Doi: <http://dx.doi.org/10.1088/1757-899X/1300/1/012022>
- [29] Malere, C.P., Donati, B., Eras, N., Silva, V.A. & Lona, L.F. 2022. Electromagnetic evaluation of radar absorbing materials based on conducting polypyrrole and organic–inorganic nanocomposite of polypyrrole/kaolinite. *J. Appl. Polym. Sci.* 139(17). 52023. Doi: <https://doi.org/10.1088/1757-899X/1300/1/012022>
- [30] Mashkoor, F., Shueb, M., Khan, M.N. & Jeong, C. 2024. Facile synthesis of Polypyrrole-decorated RGO-CuS nanocomposite for efficient nickel removal from wastewater. *Polymers.* 16(22). 3138. Doi: <https://doi.org/10.3390/polym16223138>
- [31] Meng, X., Liu, Y., Han, G., Yang, W. & Yu, Y. 2020. Three-dimensional (Fe<sub>3</sub>O<sub>4</sub>/ZnO)@ C Double-core@ shell porous nanocomposites with enhanced broadband microwave absorption. *Carbon.* 162. 356–364. Doi: <https://doi.org/10.1016/j.carbon.2020.02.035>
- [32] Ni, S., Lin, S., Pan, Q., Yang, F., Huang, K. & He, D. 2009. Hydrothermal synthesis and microwave absorption properties of Fe<sub>3</sub>O<sub>4</sub> nanocrystals. *J. Phys. D: Appl. Phys.* 42(5). 055004. Doi: <https://doi.org/10.1088/0022-3727/42/5/055004>
- [33] Ozel, E., Tuncolu, I.G., Aciksari, C. & Suvaci, E. 2016. Effect of precursor type on zinc oxide formation and morphology development during hydrothermal synthesis. *Hittite J. Sci. Eng.* 3(2). 73–80. Doi: <https://doi.org/10.17350/hise19030000034>
- [34] Pattanaik, B., & Chauhan, A. 2023. A study of stealth technology. *Mater. Today Proc.* 81. 543–546. Doi: <https://doi.org/10.1016/j.matpr.2021.03.705>
- [35] Pebrina, D. & Astuti, A. 2023. Sintesis dan karakterisasi sifat optik nanokomposit Fe<sub>3</sub>O<sub>4</sub>@ZnO:C. *Jurnal Fisika Unand.* 12(2). 298–303. Doi: <https://doi.org/10.25077/jfu.12.2.297-302.2023>
- [36] Peng, W., Han, G., Huang, Y., Cao, Y. & Song, S., 2018. Insight the effect of crystallinity of natural graphite on the electrochemical performance of reduced graphene oxide. *Results Phys.* 11. 131–137. Doi: <https://doi.org/10.1016/j.rinp.2018.08.055>
- [37] Poplavko, Y.M. 2019. Dielectrics. *Electronic Materials.* 287–408. Doi: <https://doi.org/10.1016/b978-0-12-815780-0.00007-4>
- [38] Pourbeyram, S. & Kheyri, P. 2018. Graphene/Polypyrrole nanofiber prepared by simple one step green method for

- electrochemical supercapacitors. *Synth. Met.* 238. 22–27. Doi: <https://doi.org/10.1016/j.synthmet.2018.02.002>
- [39] Rahmayanti, M. 2020. Sintesis dan karakterisasi magnetit ( $\text{Fe}_3\text{O}_4$ ): studi komparasi metode konvensional dan metode sonokimia. *Al Ulum: Jurnal Sains Dan Teknologi*. 6(1). 26-31. Doi: <http://dx.doi.org/10.31602/ajst.v6i1.3659s>
- [40] Rajan S, A., Khan, A., Asrar, S., Raza, H., Das, R.K. & Sahu, N.K. 2019. Synthesis of  $\text{ZnO}/\text{Fe}_3\text{O}_4/\text{rGO}$  nanocomposites and evaluation of antibacterial activities towards *E. coli* and *S. aureus*. *IET Nanobiotechnology*. 13(7). 682-687. Doi: <https://doi.org/10.1049/iet-nbt.2018.5330>
- [41] Ruiz-Perez, F., López-Estrada, S.M., Tolentino-Hernández, R.V. & Caballero-Briones, F. 2022. Carbon-based radar absorbing materials: A critical review. *J. Sci.: Adv. Mater. Devices*. 7(3). 100454. Doi: <https://doi.org/10.1016/j.jsamd.2022.100454>
- [42] Safitri, R.F., & Kusumawati, D.H. 2020. Aplikasi bahan komposit berbasis reduced graphene oxide (rGO). *Inovasi Fisika Indonesia*. 9(2). 93-104. Doi: <https://doi.org/10.26740/ifi.v9n2.p93-104>
- [43] Salimi, N., Mohammadi-Manesh, E., Ahmadvand, N., Danafar, H. & Ghiasvand, S. 2024. Curcumin-loaded by  $\text{Fe}_3\text{O}_4/\text{GO}$  and  $\text{Fe}_3\text{O}_4/\text{ZnO}/\text{GO}$  nanocomposites for drug delivery applications: synthesis, characterization and anticancer assessment. *J. Inorg. Organomet. Polym. Mater.* 34(3). 1256-1271. Doi: <https://doi.org/10.1007/s10904-023-02883-7>
- [44] Satria, N. & Putra, A. 2017. Synthesis and characterization of cocoa pods waste carbon for Radar Absorber Material. In 2017 Progress in Electromagnetics Research Symposium-Fall (PIERS-FALL). *IEEE*. 1532-1535. Doi: <https://doi.org/10.1109/piers-fall.2017.8293375>
- [45] Sawitri, E., Azmiyati, C. & Siahaan, P. (2018). Silica magnetite adsorbent: effect of drying temperature of silica sol gel on magnetite core structure. *Jurnal Kimia Sains Dan Aplikasi*. 21(3). 149–154. Doi: <https://doi.org/10.14710/jksa.21.3.149-154>
- [46] Shanmugam, S. & Nanjan, S. 2019. In-situ conversion of rGO from graphene oxide based on solar mediated enhanced characterization properties. *Наносистемы: Физика, Химия, Математика*. 10(5). 579–584. Doi: <https://doi.org/10.17586/2220-8054-2019-10-5-579-584>
- [47] Sudhakar, Y.N., Vindyashree, Smitha, V., Prashanthi, Poornesh, P., Ashok, R. and Selvakumar, M. 2015. Conversion of pencil graphite to graphene/polypyrrole nanofiber composite electrodes and its doping effect on the supercapacitive properties. *Polym. Eng. Sci.* 55(9). 2118-2126. Doi: <https://doi.org/10.1002/pen.24053>
- [48] Sujiono, E.H., Zabrian, D., Dahlan, M.Y., Amin, B.D. & Agus, J., 2020. Graphene oxide based coconut shell waste: synthesis by modified Hummers method and scharacterization. *Heliyon*. 6(8). e04568. Doi: <https://doi.org/10.1016/j.heliyon.2020.e04568>
- [49] Sun, W.F. & Sun, P.B. 2022. Electrical insulation and radar-wave absorption performances of nanoferrite/liquid-silicone-rubber composites. *Int. J. Mol. Sci.* 23(18). 10424. Doi: <https://doi.org/10.3390/ijms231810424>
- [50] Santamaría-Juárez, G., Gómez-Barojas, E., Quiroga-González, E., Sánchez-Mora, E., Quintana-Ruiz, M. and Santamaría-Juárez, J.D. 2020. Safer modified Hummers' method for the synthesis of graphene oxide with high quality and high yield. *Mater. Res. Express*. 6(12). 125631. Doi: <https://doi.org/10.1088/2053-1591/ab4cbf>
- [51] Syihabuddin, D.M. & Munasir, M. 2024. Green synthesis nanopartikel  $\text{Fe}_3\text{O}_4$  dengan bioreduktor ekstrak daun mimba (*Azadirachta indica*): aplikasi sebagai material fotokatalis degradasi methylene blue. *Inovasi Fisika Indonesia*. 13(3). 118–123. Doi: <https://doi.org/10.26740/ifi.v13n3.p118-123>
- [52] Taryana, Y., Manaf, A., Sudrajat, N. & Wahyu, Y. 2019. Material penyerap gelombang elektromagnetik jangkauan frekuensi radar. *Jurnal Keramik dan Gelas Indonesia*. 28(1). 1-29.
- [53] Taufantri, Y., Irdhawati, I. & Asih, I. 2016. Sintesis dan karakterisasi grafena dengan metode reduksi grafit oksida menggunakan pereduksi Zn. *Jurnal Kimia VALENSI*. 2(1). 17–23. Doi: <http://dx.doi.org/10.15408/jkv.v2i1.2233>
- [54] Tong, G., Du, F., Wu, W., Wu, R., Liu, F. & Liang, Y. 2013. Enhanced reactive oxygen species (ROS) yields and antibacterial activity of spongy  $\text{ZnO}/\text{ZnFe}_2\text{O}_4$  hybrid micro-hexahedra selectively synthesized through a versatile glucose-engineered co-precipitation/annealing process. *J. Mater. Chem. B*. 1(20). 2647-2657. Doi: <https://doi.org/10.1039/c3tb20229a>
- [55] Usvanda, L.N. & Zainuri, M. 2016. Sintesis dan karakterisasi lapisan radar absorbing material (RAM) berbahan dasar bam/pani pada rentang gelombang x-band dengan variasi ketebalan. *Jurnal Sains Dan Seni ITS*. 5(2). 129237. Doi: <http://dx.doi.org/10.12962/j23373520.v5i2.17900>
- [56] Visca, R., Dewi, M.N., Liviani, A. & Satriawan, B.D. 2022. Characterization of FTIR in graphite from palm oil waste with ferric chloride catalyst. *Interdisciplinary Social Studies*. 1(11). 1355-1358. Doi: <https://doi.org/10.55324/iss.v1i11.276>
- [57] Wang, Y., Yang, P., Zheng, L., Shi, X. & Zheng, H. 2020. Carbon nanomaterials with  $\text{sp}^2$  or/and  $\text{sp}$  hybridization in energy conversion and storage applications: A review. *Energy Storage Mater.* 26. 349-370. Doi: <https://doi.org/10.1016/j.ensm.2019.11.006>
- [58] Yogasundari, M. & Manikandan, A. 2020. Synthesis, structural, morphological and magnetic properties of  $\text{Fe}_3\text{O}_4/\text{ZnO}$  nanocomposites by co-precipitation method. *Malaya Journal of Matematik*. 1(2). 2264-2266. Doi: <https://doi.org/10.26637/MJM0S20/0582>
- [59] Xu, C., Shi, X., Ji, A., Shi, L., Zhou, C. & Cui, Y. 2015. Fabrication and characteristics of reduced graphene oxide produced with different green reductants. *PloS one*. 10(12). e0144842. Doi: <https://doi.org/10.1371/journal.pone.0144842>
- [60] Xue, J., Sun, Q., Zhang, Y., Mao, W., Li, F. and Yin, C. 2020. Preparation of a polypyrrole/graphene oxide composite electrode by electrochemical codeposition for capacitor deionization. *ACS omega*. 5(19). 10995-11004. Doi: <https://doi.org/10.1021/acsomega.0c00817>
- [61] Yang, Z., Sheng, Q., Zhang, S., Zheng, X. & Zheng, J. 2017. One-pot synthesis of  $\text{Fe}_3\text{O}_4$ /polypyrrole/graphene oxide nanocomposites for electrochemical sensing of hydrazine. *Microchim. Acta*. 184(7). 2219-2226. Doi: <https://doi.org/10.1007/s00604-017-2197-0>
- [62] Yin, P., Deng, Y., Zhang, L., Huang, J., Li, H., Li, Y., Qi, Y. & Tao, Y. 2018. The microwave absorbing properties of  $\text{ZnO}/\text{Fe}_3\text{O}_4$ /paraffin composites in low frequency band. *Mater. Res. Express*. 5(2). 026109. Doi: <https://doi.org/10.1088/2053-1591/aaae58s>
- [63] Putra, A., Yohandri, Z., Sumantyo, J.T.S. & Sanjaya, H. 2019. A low-cost radar absorber based on palm shell active carbon for anechoic chamber. *Int. J. Adv. Sci. Eng. Inf. Technol.* 9. 1976-1981. Doi: <https://doi.org/10.18517/ijaseit.9.6.9961>
- [64] Zhou, A., Yu, T., Liang, X. & Yin, S. 2023.  $\text{H}_2\text{O}_2$ -free strategy derived from Hummers method for preparing graphene oxide with high oxidation degree. *FlatChem*. 38. 100487. Doi: <https://doi.org/10.1016/j.flatc.2023.100487>
- [65] Zulpadrianto, Z., Yohandri, Y. & Putra, A. 2018. Development radar absorber material using rice husk carbon for anechoic chamber application. *IOP Conf. Ser.: Mater. Sci. Eng.* 12002. Doi: <https://doi.org/10.1088/1757-899x/335/1/012002>